Challenges of quantification of TSPO in the human brain

Rainer Hinz and Roland Boellaard

Published: 21 September 2015

by Springer

in Clinical and Translational Imaging

December 2015, Volume 3, Issue 6, pp 403-416

Challenges of quantification of TSPO in the human brain

Authors: Rainer Hinz (Wolfson Molecular Imaging Centre, University of Manchester, Manchester, UK) and Ronald Boellaard (Department of Radiology and Nuclear Medicine, VU University Medical Center, Amsterdam, The Netherlands)

Abstract

The first positron emission tomography (PET) imaging studies in humans of the translocator protein 18kDa (TSPO) were conducted in the 1980ies with a primary interest in quantifying the binding in peripheral organs such as the heart, spleen and kidneys to what was then known as the peripheral benzodiazepine receptor. However, the number of studies rapidly increased when the focus of the research shifted to the brain, and [^{11}C](*R*)-PK11195 became *de facto* the reference radiotracer for all *in vivo* TSPO binding assays. For the quantitative analysis of the data which initially was performed with compartmental models and plasma input functions, this led to the adoption of the reference tissue kinetic models which were developed at the same time in the mid 1990ies. In contrast to many neuro-receptor studies of the dopaminergic or serotonergic system, it was not possible to anatomically define a brain region devoid of TSPO that could serve as a reference region. Instead, data driven techniques were adopted that extracted at the voxel level reference tissue kinetics without incorporating anatomical information.

In this review, an overview of the development, use and challenges of the various quantitative analysis methods for TSPO brain PET data is given. The different approaches to (automatically) extract reference tissue input curves from the dynamic images are discussed. Descriptions of key PET imaging studies exploring TSPO binding quantitatively in disease populations are included.

Keywords: Positron Emission Tomography (PET), Quantification, [^{11}C]PK11195, Translocator Protein 18kDa (TSPO)

Abbreviations:

AD Alzheimer's disease
B_{avail} density of available sites available to bind radioligand *in vivo*
BBB blood-brain barrier
BF blood flow
BP binding potential
BP_F binding potential relative to the free ligand concentration in plasma
BP_{ND} binding potential relative to the non-displaceable binding in tissue
CBF cerebral blood flow
CNS central nervous system
CT computed tomography
HAB high-affinity binder
HD Huntington's Disease
HPLC high-performance liquid chromatographic
HHRT High Resolution Research Tomograph
INMiND Imaging of Neuroinflammation in Neurodegenerative Diseases
K_D dissociation constant
LAB low-affinity binder
MAB mixed affinity binder
MCI mild cognitive impairment
MRI magnetic resonance imaging
PET positron emission tomography
PK11195 1-(2-chlorophenyl)-*N*-methyl-*N*-(1-methylpropyl)-3-isoquinolinecarboxamide
PVE partial volume effect
ROI region of interest
SPE solid phase extraction
SRTM simplified reference tissue model
SRTMV simplified reference tissue model with vascular component
SUV standard uptake value
SVCA4 supervised cluster analysis with four kinetic classes
SVCA6 supervised cluster analysis with six kinetic classes
TAC time-activity curve
TLC thin-layer chromatography
TSPO translocator protein 18 kDa
V_{ND} non-displaceable volume of distribution
V_T total volume of distribution

Introduction

The translocator protein 18 kDa (TSPO) is a nuclear encoded mitochondrial protein which is abundant in peripheral organs (particularly adrenal glands and kidney) and haematogenous cells. Its function still needs full elucidation but it plays an important role in steroid synthesis and in the regulation of immunological responses in mononuclear phagocytes. In diseases of the central nervous system (CNS), high levels of TSPO have been observed in infiltrating blood-borne cells and in activated microglia. Significant microglial activation occurs after mild to severe neuronal damage resulting from traumatic, inflammatory, degenerative and neoplastic disease. Microglia are activated in the surroundings of focal lesions but also in the distant, anterograde and retrograde projection areas of the lesioned neural pathway.

The best-characterised ligand of TSPO is 1-(2-chlorophenyl)-*N*-methyl-*N*-(1-methylpropyl)-3-isoquinolinecarboxamide or PK11195 which binds to TSPO with nanomolar affinity in many species. At the time of writing, entering the term PK11195 into the PubMed search engine returned almost 1,300 literature references. The first seven papers with reference to PK11195 were published in 1983, thereafter the number of publications grew year by year to around 50 in 1989. From then, the publication output has been almost constant at a rate of approximately 50 papers a year for the last 25 years.

The first positron emission tomography (PET) imaging study with ^{11}C-labelled PK11195 was reported in 1986 [1]. In contrast to later studies using enantiomerically pure (*R*)-PK11195, all early work was carried out with racemic PK11195. Stereoisomerism however does not affect physical properties of the compound such as lipophilicity, therefore does not impact on the passage across the blood-brain barrier (BBB) by passive diffusion. In [1], the specificity of [^{11}C]PK11195 binding to TSPO in the canine heart was demonstrated through the inhibition of [^{11}C]PK11195 binding by an excess of several agonists or antagonists of what was then known as central or peripheral-type benzodiazepine receptors. The distribution and specificity of [^{11}C]PK11195 was similar in dogs and in humans. In the human studies, the injection of various amounts of unlabelled PK11195 (100, 200 or 500 µg / kg body weight) 30 min after injection of [^{11}C]PK11195 led to a rapid decrease in radioactivity in the heart. A linear correlation was demonstrated between the concentration of PK11195 in the human heart (expressed as pmol/cm^3) and the amount of PK11195 injected for doses below 3 nmol / kg.

Efforts to label Ro 5-4864 (a peripheral inverse agonist) with ^{11}C for use in PET imaging did not result in a radiotracer superior to [^{11}C]PK11195 [2,3]. These human studies were conducted in brain tumours introducing TSPO ligands to brain imaging. The study by Junk *et al*. acquired dynamic PET data over 80 min after injection of an [^{11}C]Ro 5-4864 or an [^{11}C]PK11195 bolus together with arterial plasma input functions. Local blood flow (BF) was also measured with [^{15}O]H_2O PET [3]. Compartmental modelling employing nonlinear least squares fitting was used to estimate regional transfer constants K_1 (expressed in ml·g^{-1}·min^{-1}) for the passage of [^{11}C]PK11195 from blood to tissue. Together with the regional BF (expressed in ml·g^{-1}·min^{-1}) estimates, the percentage unidirectional extraction of

[^{11}C]PK11195 in the different tissue classes was calculated. For the four patients scanned with [^{11}C]PK11195, the mean ± standard deviation were [3]

- Tumour K_1= 0.027 ± 0.014, BF= 0.40 ± 0.17, Extraction= 7.5 ± 4.4 %
- Grey matter K_1= 0.028 ± 0.011, BF= 0.55 ± 0.06, Extraction= 4.9 ± 1.4 %
- White matter K_1= 0.013 ± 0.007, BF= 0.28 ± 0.08, Extraction= 4.4 ± 1.7 %

The authors concluded that the high [^{11}C]PK11195 radioactivity in non-contrast-enhancing glioma and the nearly equal K_1 values in tumour and remote grey matter indicated that disruption of the blood-brain barrier was not the basis for the positive imaging results [3]. The strong correlations observed between specific activity and tumour radioactivity suggested that most of the binding sites were occupied at the lower specific activities, and supported the view that the increased radioactivity in tumour is due to high-affinity binding to TSPO [3].

In a subsequent brain imaging study of after ischaemic stroke [4], sequential cerebral blood flow (CBF) measurements, contrast-enhanced computed tomography (CT) and 60 min dynamic PET following [^{11}C]PK11195 bolus injection were performed 6, 13 and 20 days after the event. There was no obvious relation between CBF and retention of [^{11}C]-PK11195 [4]. Although the authors reported that ^{11}C radioactivity and regions of contrast enhancement in the CT did not match closely, the retention of radioactivity was expressed as average counts/s per ml brain tissue 40-60 min post-injection relative to the integral (0-50 min) of radioactivity in metabolite-corrected plasma [4]. From a quantification point of view, this approach avoided any assumption regarding integrity of the BBB. It was concluded that TSPO PET can be used to detect the anatomical localisation *in vivo* of the accumulation of macrophages and that the temporal profile of this response in brain lesions can be monitored [4].

Reference region analyses

In the 1990ies the concept of expressing the binding of the radiotracer in the region with high target expression relative to another region with low specific binding or 'reference region' was introduced into PET data analysis and very rapidly gained popularity in neuro-receptor imaging. Milestones of these developments were the works by Blomqvist *et al.* [5], Cunningham *et al.* [6], Lammertsma *et al.* [7,8] and Logan *et al.* [9]. From a practical point of view, this approach provided the huge advantage of avoiding the need for blood sampling during the PET scan. This not only reduced the discomfort to the study participants and increased the feasibility of longitudinal studies with repeat scans but it also overcame the need for radio-analytical methods to accurately identify the plasma metabolite fractions in the samples taken thus potentially lower the variability in the data acquired in different laboratories.

Parent fraction determination in plasma samples

Pike *et al.* reported in 1993 that in a study of 10 patients with cardiac embolic infarcts and 5 patients with multiple sclerosis, the fraction of unchanged radioligand was 83 ± 8 % at 5 min and 55 ± 7 % at 60 min (mean ± standard deviation) following administration of [*N*-methyl-^{11}C]PK11195 [10]. They used an automated technique combining solid phase extraction (SPE) with reverse phase high-performance liquid chromatography (HPLC) that had previously been developed for the routine determination in plasma of unchanged ^{11}C labelled radioligands [10]. A rapid HPLC procedure for the quantitative determination of [^{11}C]PK11195 in mouse plasma and tissue and in human plasma was described by De Vos *et al.* in 1999 [11]. After intravenous injection of 370 MBq in five human volunteers, the unchanged fraction of [^{11}C]PK11195 in human plasma was found to be 95 ± 1 % at 5 min, 78 ± 3.3 % at 20 min and 66 ± 2.9 % at 35 min (mean ± standard deviation) [11]. Subsequently, the HPLC procedure with online SPE was modified for analysing [^{11}C](*R*)-PK11195 plasma samples, yielding total sample recoveries of more than 98% [12]. Whilst this refined method effectively reproduced the parent fraction previously reported at 5 min in [10], the percentage of unchanged radioligand in plasma was lower than in [11] with 57.5 ± 6.4 % at 20 min and 45.2 ± 9.4 % at 60 min (mean ± standard deviation, 10 human subjects) [12]. It is important to notice that beginning with [12] the racemic mixture [^{11}C]PK11195 has been replaced with enantiomerically pure [^{11}C](*R*)-PK11195 after the discovery of significantly higher retention of the *R*-enantiomer than the *S*-enantiomer in focal cortical lesions in the rat [13, 14].

Roivainen *et al.* developed a fast and reliable high performance liquid chromatography (radio-HPLC) method with online radioactivity measurement and a thin-layer chromatography (radio-TLC) method combined with digital photostimulated luminescence autoradiography for the quantitation of [^{11}C](*R*)-PK11195 and its radioactive metabolites in sequential plasma samples drawn during PET imaging [15]. In order to evaluate the reproducibility of radio-HPLC metabolite analyses, ten patients with Alzheimer's disease (AD) underwent two successive [^{11}C](*R*)-PK11195 examinations on separate days. Consistent with the previous report by Greuter *et al.* [12], large between subject variation in the metabolism of [^{11}C](*R*)-PK11195 was found [15]. The level of unmetabolised [^{11}C](*R*)-

PK11195 decreased slowly from 96.3 ± 1.6 % at 5 min, 76.2 ± 6.1 % at 20 min to 57.8 ± 10.9 % at 50 min after injection (mean ± standard deviation) [15]. The radio-HPLC method was deemed to be of moderate to high reliability with intraclass correlation coefficients (ICC) ranging between 0.41 and 0.80 on the measurements at time points from 5 to 40 min. It was reported that data from radio-TLC correlated well with those from radio-HPLC albeit the radio-HPLC method was found to be slightly more sensitive and to yield a better separation between [^{11}C](*R*)-PK11195 and its metabolites than the radio-TLC method [15].

In another test-retest study, performed by Jučaite *et al.* in a cohort of six control subjects, the unchanged fraction of [^{11}C](*R*)-PK11195 in plasma declined only to 70 ± 1.5 % (mean ± standard deviation, range: 60 to 77 %) at 50 min after injection [16], which are the highest parent fraction values reported in the literature. At the other end of the spectrum, Lamare *et al.* reported parent fractions in plasma as low as 68.0 ± 6.6% at 5 min and 29.1% ± 5.7% at 60 min after injection [17]. The study was conducted in seven patients with systemic inflammatory disorders and, in contrast to all reports previously quoted, arterialised venous samples from a heated arm or hand were analysed [17]. Thus it is possible that the comparatively low parent fractions in [17] are actually a reflection of differences in the fractions of [^{11}C](*R*)-PK11195 between arterial and arterialised venous blood although an investigation with concomitant arterial and arterialised venous sampling would be needed for confirmation. Another possibility for the fast *in vivo* metabolism of [^{11}C](*R*)-PK11195 seen in study [17] could be the inclusion of patients with systemic inflammatory disorders. A side by side comparison of parent fractions in plasma reported by selected studies can be looked up in Table 3 of Roivainen *et al.* [15].

This short discourse on the challenges presented by the determination of the fractions of radioactivity due to [^{11}C](*R*)-PK11195 in human plasma samples (that equally apply to blood and tissue samples in pre-clinical research studies with usually even smaller sized samples and lower activity levels in small laboratory animals) makes the desire to employ a bloodless quantification method all too understandable. One of the first such publications with [^{11}C]PK11195 came out in 1995 by Groom *et al.* [18]. In short:

- Eight patients with a diagnosis of probable AD underwent PET of the brain using [^{11}C]PK11195.
- Uptake of [^{11}C]PK11195 in various brain regions was expressed relative to that in the cerebellum
- and compared to values determined in one normal elderly subject and in clinically and anatomically unaffected hemispheres of seven patients with small unilateral gliomas.
- No increases in peripheral benzodiazepine binding were identified in patients with probable AD [18].

The paper concluded that the peripheral benzodiazepine binding sites associated with microgliosis and cellular inflammation in AD at *post mortem* were undetectable by PET using [^{11}C]PK11195 in patients with mild-to-moderate dementia [18].

It is worth to go through the individual points of the methodology used in this investigation to discuss whether the conclusion was actually derived on solid grounds.

First, it had been established before that in AD an inflammatory process occured in the plaques and that activated microglial cells expressing certain monocyte/macrophage markers were present, as reviewed for example in [19, 20]. Thus the question was whether [^{11}C]PK11195 PET provided a tool sensitive enough to detect these changes *in vivo* already at a mild-to-moderate disease stage.

Second, as to the image quantification, anatomically-configured regions of interest (ROIs) were superimposed on the images that were collected from 40 to 60 min after [^{11}C]PK11195 bolus injection and average counts per voxel were recorded [18]. To control for differences in arterial tracer activities, these ROI values were then normalised to those of the cerebellum, as studies had shown this to be one of the least pathologically affected brain structures in AD [18]. Two particular questions arise in this section:

a) Is cerebellum an appropriate choice for a reference region?
b) Can the specific binding of the radiotracer to the target TSPO be characterised well by a 40 to 60 min target-to-reference region activity ratio?

Cerebellum as an anatomically defined reference region

A reference region for the quantification of reversibly binding receptor ligands should be devoid (or almost devoid) of specific ligand binding and only share the same free and non-specific binding with the region expressing the target [6]. Furthermore, in a case-control study, the reference region should remain unaffected by the disease.

Doble *et al.* described the labelling of TSPO in *post mortem* human brains removed at autopsy from road accident victims (a woman aged 40 and two men, one aged 46 and the other 42) with racemic [^{3}H]PK11195 [21]. In quantitative autoradiographic studies, brain sections incubated in the presence of 2 nM [^{3}H]PK11195 demonstrated a heterogeneous distribution of binding sites, although the non-specific binding of [^{3}H]PK11195 was distributed uniformly: this represented 250 fmol / mg protein (grey matter) and 150 fmol / mg protein (white matter) [21]. The specific [^{3}H]PK11195 binding sites were present in the grey matter whilst the white matter contained only non-specific binding [21]. For the cerebellar cortex, binding densities of 660 ± 85 fmol / mg protein for the granular cell layer, 191 ± 55 fmol / mg protein for the molecular cell layer and 41 ± 32 fmol / mg protein for white matter were reported [21]. For comparison, the highest binding densities were found in the dorsomedial thalamic nucleus (1912 ± 412 fmol / mg protein) and in inferior olivary nucleus of the medulla (1655 ± 355 fmol / mg protein) [21]. Moderate binding densities were reported for the cortex: 726 ± 128 fmol / mg protein for the cingulate gyrus, 886 ± 108 fmol / mg protein for the insula and 892 ± 113 fmol / mg protein for the orbital gyrus [21]. In summary, specific [^{3}H]PK11195 binding in *post mortem* human brain sections was lower in cerebellar grey matter than in cortical grey matter or the diencephalic structures. However, the cerebellar grey matter was not free of specific [^{3}H]PK11195 binding.

How does this distribution of TSPO in healthy human brain translate into an *in vivo* PET imaging study? Owen *et al.* performed a human TSPO blocking study with the radioligand [^{11}C]PBR28 and the selective TSPO antagonist XBD173 [22]. Note, that [^{11}C]PBR28 binds to TSPO in human brain from different subjects in one of three ways: high-affinity binders and low-affinity binders (HABs and LABs) express a single binding site for TSPO with either high or low affinity, respectively, whereas mixed affinity binders (MABs) express approximately equal numbers of the HAB and LAB binding sites [23]. The TSPO binding phenotype is determined by the polymorphism rs6971 located in exon 4 of the TSPO gene resulting in a non-conservative amino-acid substitution at position 147 from alanine to threonine (Ala147Thr) in the fifth transmembrane domain of the TSPO protein [23]. In the TSPO blocking study, six healthy volunteers (all of them HABs) underwent paired [^{11}C]PBR28 PET scanning with arterial sampling [22]. The baseline scan was with tracer alone whereas the repeat scan was performed two hours after an oral dose of XBD173 (10 to 90 mg). The non-displaceable volume of distribution V_{ND} was then estimated via an occupancy plot [24, 25]. The group average V_{ND} was reported as 1.89 (95% confidence interval 1.32, 2.46) with an overall whole-brain total volume of distribution V_T in HAB of 4.33 ± 0.29 [23]. The figure provided in [23] indicated that the V_T in the cerebellum was slightly below this whole-brain V_T which still is about twice the V_{ND}. In summary, Owen *et al.* found that about half of the [^{11}C]PBR28 total volume of distribution V_T in the cerebellum was attributable to displaceable binding [23].

Taken these findings together, great caution is warranted for the use of cerebellum as a pseudo-reference tissue because the amount of specific binding in the cerebellar grey matter of healthy human brain was non-negligible. A negative bias, i.e. an underestimation of the true specific binding in the target region, is to be expected if the cerebellum is used as a reference region. If the specific binding in the ROI is smaller than that in the cerebellum, even apparently negative specific binding could be the consequence.

Target-to-reference ratio as outcome measure for specific binding

Which mathematical approach should be used to work out the specific binding of a PET receptor ligand *in vivo*? The standard model for the quantification of the interaction between binding sites and reversibly binding ligands in PET was introduced in 1984 by Mintun *et al.* [26]. It was based on a three-tissue compartment model with separate compartments for free, non-specifically bound and specifically bound ligand in brain tissue [26]. It also introduced the new term binding potential, equal to the product of the density of available binding sites B_{avail} with the binding affinity K_D^{-1}, to express specific binding of a receptor ligand *in vivo* [26]. After the consensus nomenclature for *in vivo* imaging of reversibly binding radioligands was agreed in 2007 [27], this binding potential BP_F expressed the size of the compartment for specific binding relative to the free ligand concentration in plasma. Another variant of the binding potential is BP_{ND} denoting the specific binding relative to the non-displaceable binding which is represented by the combined free and non-specifically bound compartment [28].

At true equilibrium, V_T is the ratio of the total tissue concentration to the concentration of parent compound in arterial plasma. Equilibrium conditions can be achieved by continuous infusion of the radiotracer, which often follows after an initial loading bolus [29]. With the availability of a reference region free of specific binding and the uniformity of the free and non-specific binding, the binding potential BP_{ND} can be calculated from the ratio of the concentration in the ROI over the concentration in the reference region minus one at true equilibrium.

True equilibrium cannot be reached after a single bolus injection. Often, however, the tissue concentration cleared at the same rate as the parent concentration in plasma from a certain time after bolus injection onwards which meant that a plot of the ratio of tissue concentration over metabolite corrected plasma concentration reaches a plateau. Following the terminology of parent-daughter decay in radiation physics, this condition is referred to as transient equilibrium [29, 30]. An apparent BP_{ND} calculated from the ratio of the concentration in the ROI over the concentration in the reference region minus one at transient equilibrium, however, is in general different from the true BP_{ND} [31]. The magnitude of that difference depends on the clearance rates in the ROI and the reference region, respectively, and on the time point the ratio is calculated [29, 31]. To avoid subjecting the results of a research study to these uncertainties associated with simple tissue concentration ratios, a model based kinetic or graphical analysis of the data acquired after bolus injection is the preferred strategy to derive binding parameters [32].

Returning to the points raised about the methodology used in [18], the third item on the list is now considered which is the appropriate choice of the control population in a case-control study. After Hanahan and Weinberg highlighted the role of inflammation in inducing many types of cancer by adding tumour-promoting inflammation as an enabling characteristic [33] to the previously described six hallmarks of cancer [34], it is now widely recognised that inflammation is evident at the earliest stages of neoplastic disease. Therefore it can be questioned whether seven patients with small unilateral gliomas are a suitable control cohort to assess whether neuro-inflammation is detectable in AD patients with mild-to-moderate dementia using [^{11}C]PK11195 PET [18]. Although control values were derived from the clinically and anatomically unaffected hemispheres of the cancer patients, the possibility of pathologically raised [^{11}C]PK11195 binding in the contralateral hemispheres cannot be rejected. If this had been the case, a comparison of the [^{11}C]PK11195 binding between the contralateral hemispheres of the glioma patients and the AD patients might have missed the neuro-inflammation if it had been present in the AD cohort. Therefore it is generally preferred to use age matched healthy participants as reference population in TSPO imaging studies with a case-control design.

Taken all the methodological points analysed together, the structure of the study presented in [18] had several methodological shortcomings affecting the ability to identify increases in TSPO binding in patients with probable AD. In contrast, a subsequent study by Cagnin *et al.* found activated microglia measured *in vivo* with [^{11}C](*R*)-PK11195 PET in dementia [35]. A comparison between 15 normal individuals (age 32-80 years), eight patients with AD, and one patient with minimal cognitive impairment was performed. Parametric

images of regional [^{11}C](*R*)-PK11195 binding potential were generated with a basis-function implementation of the simplified reference tissue model (SRTM) [8,36]. For the extraction of the reference tissue kinetics from the dynamic images, no anatomically defined brain region was used. Instead, a data driven technique was adapted to dynamic [^{11}C](*R*)-PK11195 brain PET data to generate a reference input function. Two main findings were reported in [35]:

- In normal individuals, regional [^{11}C](*R*)-PK11195 binding did not significantly change with age, except in the thalamus, where an age-dependent increase was found.
- Patients with AD showed significantly increased regional [^{11}C](*R*)-PK11195 binding in the entorhinal, temporoparietal, and cingulate cortex.

Two other technical improvements affecting signal detectability should also be mentioned. The racemic [^{11}C]PK11195 used in [18] was superseded by [^{11}C](*R*)-PK11195 in [35] as the radioligand with higher specific binding [13]. The positron camera in [35] was operated in three-dimensional acquisition mode providing both a larger axial field-of-view and increased sensitivity than the scanner with only eight rings used in [18].

Data driven methods for the extraction of reference tissue kinetics

What are data driven methods that can segment dynamic PET data into kinetic classes? In nuclear medicine data analysis, voxels in three-dimensional space are usually grouped together in ROIs based on their proximity. ROIs are directly placed on the PET images often aided by images provided by modalities with superior spatial resolution and higher tissue contrast like CT or magnetic resonance imaging (MRI). One of the problems with this approach is that it does not take into consideration the higher partial volume effect present in the nuclear medicine images due to their lower spatial resolution. It also neglects any heterogeneity within the ROI by assuming that all time-activity curves (TACs) of the voxels in one ROI were generated by one underlying kinetic process and that the variability between the voxel TACs of one ROI is only due to random statistical noise [37].

A different approach is to group voxels together based on their similarity between the voxel TACs. This means that not voxels that are close to each other in space but voxel that share similar kinetics in time will be in the same class. For example, in a dynamic PET data set that has been reconstructed in n temporal frames, each TAC consists of n measured data points. Note that the independent variable representing the time points of the TAC is usually not equidistantly spaced as the lengths of the frames tend to increase with scan time to achieve a comparable number of counts per frame compensating for the decay of the radiolabel as the scan progresses and to account for any initially fast and later slower kinetics of the radiotracer. The dependent variable is then an n-dimensional vector representing the activity concentration for each of the voxels. Now the entire set of measured voxel TACs can be partitioned or segmented into k clusters by

- defining a distance measure between two data vectors in n-dimensional space and
- calculating the distance between the cluster's centroid and the voxel's data vector.

If the distance can be transformed into an expression of the likelihood of the voxel belonging to a cluster, then this approach is referred to as 'soft clustering' because it defines a relationship for each of the voxels with all of the k clusters. This is the opposite to 'hard clustering' where each voxel is assigned to exactly one of the k clusters, the cluster whose centroid has the shortest distance to the voxel's data vector.

The squared Euclidean distance or the Mahalanobis distance [38] are two examples of distance measures used with PET data of inherently statistical nature as result of radioactive decay. The number of classes k has to be defined prior to performing the cluster analysis although it is possible to perform several cluster analysis runs across a range of values for k for example k= 2, 3, …, 12. Visualisation tools such as silhouette plots can be used to examine the tightness and separation of the classes in search for the choice of a single k [39]. If the centroid of a cluster is calculated from the voxels in the cluster, for example as the arithmetic mean or the median, then this is also referred to as 'unsupervised clustering'. If the cluster centroids are pre-defined then a 'supervised clustering' method is used.

Among the first reports of applying multivariate data analysis techniques to dynamic PET images was that by O'Sullivan in an effort to address the challenges of ROI

heterogeneity and high noise at the voxel level [40]. A mixture analysis approach was presented approximating voxel TACs as a linear combination of a number of underlying model sub-TACs [40]. Thereafter, Ashburner *et al.* described a clustering technique that adapted a mixture model to accommodate dynamic PET data [41]. The principal difference to the original algorithm was described as being concerned with the shapes of the voxel TACs (vectors) and not their absolute scaling as in dynamic PET data the observed absolute scaling is determined by the delivery of the tracer [41]. The modified algorithm was presented as being able to suppress the domination by effects of magnitude and to classify the TACs by more subtle variation in curve shapes [41]. As a consequence of the modifications, the dimensionality of the problem was reduced because all the data were effectively mapped to the same hyperplane [41]. Examples of application to [^{11}C]flumazenil brain data were given illustrating the use to partition dynamic images into areas of distinct kinetics [41].

The first report to use a data driven method for the extraction of reference tissue kinetics from dynamic [^{11}C]PK11195 brain scans was by Myers *et al.* involving control subjects and patients with Bell's Palsy, a condition where the focus of injury in the brain is confined to the facial nucleus in the brain stem [42]. The dynamic data were segmented into k= 10 clusters using the previously developed method by Ashburner *et al.* [41]. It was reported that for most subjects one of the two dominant clusters was found to represent normal kinetics, as determined by comparison of the shape of the TAC with that from control brains [42]. The TAC from this 'normal' cluster was then applied as the input function to the SRTM generating parametric maps of BP_{ND} [36].

This package of novel methodology consisting of the unsupervised cluster analysis for the extraction of reference tissue kinetics, the SRTM and its basis function implementation for the generation of parametric maps of BP_{ND} paved the way to a number of subsequent clinical research studies with [^{11}C](*R*)-PK11195. Two of those reports are of interest here as they provide more detail about the kinetic modelling and analysis [43, 44].

In the first report, 14 (8 male / 6 female) healthy subjects between the ages of 32 and 80 years (mean age 57.3 years) were studied [43]. In normal brain, the majority (around 90%) of the voxels were segmented into two clusters, one representing the TAC mainly from the skull and scalp and one representing the TAC of voxels mostly located in the cerebral cortex. The latter was identified as the kinetic of the ligand in normal brain tissue. A normalised mean TAC (population input kinetic) was calculated from the normal ligand kinetics (from each of the 14 subjects) as previously identified by cluster analysis. The suitability of the TAC extracted by cluster analysis as the individual normal ligand kinetic was confirmed by testing for dissimilarity with the normal population input kinetic (χ^2 test < 0.95) [43].

In the second report, 12 (4 male / 8 female) patients with multiple sclerosis between the ages of 28 and 66 years (mean age 46.3 years) were studied [44]. Because of the often widespread tissue pathology in multiple sclerosis, the approach presented in the first report [43] was used to extract the reference tissue TAC. Increased TSPO expression was demonstrated in areas of focal pathology and also in normal-appearing structures, including cerebral grey matter [44]. However, one patient with secondary progressive multiple sclerosis

had to be excluded from the study since no appropriate TAC could be extracted to serve as an input function [44]. Another report applying this unsupervised cluster analysis to [^{11}C](*R*)-PK11195 brain scans of 39 subjects - young and older healthy subjects, patients with amnestic Mild Cognitive Impairment (MCI) and AD patients - observed four cases where no meaningful clustering was obtained and thus these scans had to be excluded from the comparative analysis [45]. This apparent failure of the unsupervised clustering reported in several cases constituted a serious limitation of the data analysis method. How could cluster analysis be performed differently in order to always produce a TAC representing reference tissue kinetics?

Turkheimer *et al.* [46] presented a supervised cluster analysis approach [47] expressing each voxel TAC, after normalisation of each frame of the dynamic image by subtracting its mean and dividing it by its standard deviation, as a weighted linear combination of a set of six pre-defined kinetic classes. The non-negative least squares (NNLS) algorithm [48] was used to determine the set of non-negative weights per voxel, a concept similar to that underlying spectral analysis of dynamic PET data [49], resulting in a set of six parametric maps of weights for the following classes: 'normal grey matter', 'white matter', 'pathologic TSPO binding', 'blood pool', 'muscle' and 'skull' [46]. The reference tissue TAC was finally calculated as a weighted average of the original voxels TACs using the weights of the 'normal grey matter' class [46].

As the training data set for all kinetic classes except 'pathologic TSPO binding', scans of 12 control subjects acquired on the ECAT EXACT 3D were used [46]. Grey and white matter maps were obtained from the segmented MRI volume and then thresholded (only map values > 90% of maximum value were retained) to minimise the effect of partial volume [46]. ROIs for the 'blood pool' were manually placed on the venous sinus, for 'muscle' on the sternomastoid muscle and for the 'skull' on the skull [46]. The kinetic class 'pathologic TSPO binding' was defined by an ROI placed on the striatum and globus pallidus of three symptomatic patients with genetically proven Huntington's Disease (HD) [46]. The normalised TACs extracted from the scans for each kinetic class were then averaged to form the population data base needed for the supervised cluster analysis with six kinetic classes (SVCA6).

Note that due to the specific properties of the cameras, for example sensitivity, scatter fraction and spatial resolution, and the image reconstruction, for example filtered back projection or ordered subset expectation maximisation iterative method, used, SVCA6 population data bases were subsequently generated for the High Resolution Research Tomograph (HHRT) [50] using data from subjects with multiple identified risk factors of stroke but no evidence of cerebral damage [51] and for the ECAT EXACT HR+ scanner using data from patients after traumatic brain injury (TBI) [52, 53] for the definition of the 'pathologic TSPO binding' class. In fact, it was even possible to extend the SVCA approach [46] to a small animal camera with only three kinetic classes distinguishable in rat brain [54].

Su *et al.* performed a systematic comparison between the cerebellar grey matter input function and the SVCA6 generated reference tissue input function in a study on the HRRT

that involved 23 glioma patients (16 male / 7 female, age range 22 - 73 years, mean age 40 years) and 10 healthy control participants (7 male / 3 female, age range 23 - 68 years, mean age 44 years) with [^{11}C](*R*)-PK11195 [55]. Although the shapes of the two reference tissue input functions systematically differed in that the SVCA6 reference tissue input function had a higher signal in the initial phase of the scan (for the first 20 minutes or so), consistent BP_{ND} parametric maps generated with the SRTM were obtained in all control subjects and 10 of the glioma patients [55]. However, in the remaining 13 glioma scans, BP_{ND} from SVCA6 reference tissue input and BP_{ND} from cerebellar grey matter input were still highly correlated but BP_{ND} from SVCA6 reference tissue input were systematically smaller than BP_{ND} from cerebellar grey matter input throughout the brain both inside and outside the tumours [55]. In those scans, the TAC of the SVCA6 reference tissue input function was higher than the cerebellar grey matter TAC throughout the entire duration of the 60 min dynamic PET scan. This observation led to the hypothesis that in some instances the 'normal grey matter' class of SVCA6 on the HRRT may be contaminated by high binding in the connective tissue outside the brain or in the venous sinuses [56]. This possible vulnerability of the SVCA6 generated reference tissue input function on the HRRT was further supported by the report of a 78 year old control participant with generalised brain atrophy on the MRI where the BP_{ND} with SVCA6 reference tissue input were higher than the BP_{ND} with cerebellar grey matter input throughout the brain [56].

An alternative approach applying a brain mask (usually obtained from a co-registered structural brain MRI) to the dynamic [^{11}C](*R*)-PK11195 image prior to performing the supervised cluster analysis was devised [52, 57], classifying the data in only four clusters. Thus the number of weights per voxel to be estimated was reduced from 6 to 4, and extra-cerebral signal of the bone and soft tissue classes was eliminated from the classification process [52, 57].

An evaluation of this supervised cluster analysis with four kinetic classes (SVCA4) was reported from [^{11}C](*R*)-PK11195 scans of 39 subjects - young and older healthy subjects, MCI and AD patients - acquired on the ECAT EXACT HR+ camera [57]. The SVCA4 reference tissue input provided the best contrast between subject groups compared with SVCA6 input and cerebellar input [57] (Figure 1). Estimating the V_T of the three reference tissue TACs (cerebellum, SVCA6 and SVCA4) using the reversible two tissue compartment, four rate constants model with metabolite corrected arterial plasma input function, the median V_T in each of the four groups studied was smallest for SVCA4 suggesting that of those three reference input functions the SVCA4 reference tissue input came closest to the TAC only representing the non-displaceable binding [57]. Consequently, SVCA4 provided the highest target region BP_{ND} values when the reference input functions were used with the SRTM [57] (Figure 1).

Refinements of the reference tissue model and relationship with age

This touches on another important point that of the very small values of BP_{ND} obtained with the SRTM and a reference input function, and even the occurence of negative values on the parametric images for BP_{ND}. Kropholler *et al.* [58] pointed out that the mean regional BP_{ND} obtained with the SRTM reported in [35] ranged from 0.07 to 0.46 whereas in their own [^{11}C](*R*)-PK11195 study with a similar population consisting of healthy controls, MCI and AD patients the whole cortex BP_{ND} was 1.6 ± 0.4 using the plasma input reversible two-tissue compartment model with four rate constants and a blood volume fraction correction [58]. Subsequently, the authors developed a simplified reference tissue model with correction for non-specific binding using a plasma input model with two compartments for the reference tissue [59]. The BP_{ND} estimates with that model approximately doubled relative to the BP_{ND} estimates obtained with the SRTM but were still significantly lower than those provided by the two-tissue reversible plasma input model [59]. The large discrepancy between plasma input model derived BP_{ND} versus those obtained using this or the original reference tissue model were thought to result from a large contribution of specific binding in the reference region used and/or from signal arising from the vasculature.

Subsequently, Tomasi *et al.* applied the simplified reference tissue model which accounts for tracer vascular activity (SRTMV) to dynamic [^{11}C](*R*)-PK11195 brain scans acquired on the ECAT EXACT 3D [60]. This variation of the SRTM had previously been developed for the analysis of dynamic data for the serotonin 5-HT$_{1A}$ receptor ligand [*carbonyl*-^{11}C]WAY-100635, a tracer characterised by low signal in the reference tissue during late time of the scans relative to the activity in the vasculature [61]. Therefore, a significant proportion of the TAC at late time is not reflecting tissue activity but spill-over of vascular activity. The SRTM in its original form [8, 36] does not account for vascular signal neither in the reference nor the target region resulting in parameter bias dependent on the specific properties of the radiotracer and the study population. In the case of neurodegenerative disease, changes in blood volume and TSPO expression in the vasculature were reported [60]. The substitution of the SRTM with the SRTMV resulted in an increase of BP_{ND} in both AD patients and age-matched healthy controls [60]. Comparing the estimates of the regional fractional blood volumes obtained with the SRTMV, the AD patients had lower values in all brain regions examined than the healthy controls [60].

An overall visual comparison between SRTM and SRTMV using either cerebellum, SVCA6 or SVCA4 to provide a reference input function for parametric mapping in an AD subject scanned with [^{11}C](*R*)-PK11195 on the ECAT EXACT HR+ camera is shown in Figure 2 [57]. Selecting the thalamus as example target ROI, in Figure 1 findings in three cohorts (young controls, old controls and AD patients) are compared for the same combinations of models and reference input as in Figure 2. Taking the increase in grey matter to white matter contrast provided by the inclusion of the target region blood volume variable in the SRTMV into consideration, Yaqub *et al.* concluded that for [^{11}C](*R*)-PK11195 data acquired on the ECAT EXACT HR+ the SRTMV in combination with the SVCA4 reference input provided the best contrast between groups [57].

Another proposal to modify the strategy of quantification of specific TSPO binding was presented by Rizzo *et al.* for scans with [^{11}C]PBR28 [62]. In parallel to the reversible two tissue compartment, four rate constants model for the description of the tracer kinetics in tissue [16, 58] another compartment with only a single rate constant was added for the slow apparently irreversible uptake of [^{11}C]PBR28 into the vessels [62]. Data from 19 healthy participants (10 MAB, 8 HAB, 1 with unknown binding affinity status) were analysed and improved quality of the fitted tissue TACs, in particular during the first 5 minutes of the scan, were reported [62]. The total volumes of distribution V_T estimated with the modified model were more than three-fold smaller but the V_T group difference between MABs and HABs increased from 39 % to 57 % with the modified model [62]. Further validation of this approach in clinical populations and with other TSPO tracers is pending, and a bloodless model implementation would facilitate its acceptance in larger studies.

The attempt made in [62] to kinetically separate the specific binding of the radioligands to TSPO in brain tissue from that to TSPO localised in the endothelium of brain vessels is relevant to discuss the inconsistent findings in the literature on the relationship between age and BP_{ND} in healthy subjects. The first two reports using the SRTM together with either a cerebellar input function or an unsupervised cluster analysis input function by Cagnin *et al.* found an age-related increase of [^{11}C](*R*)-PK11195 BP_{ND} only in the thalamus but not in the temporal lobe of 14 (8 male / 6 female) healthy subjects between the ages of 32 and 80 years (mean age 57.3 years) [43,35].

In another study [63], a normalised input curve was first created by averaging the ROIs placed over the cerebral cortical regions including the frontal, parietal, and occipital cortices in a healthy group. This population reference input curve was then used with the SRTM to quantify the [^{11}C](*R*)-PK11195 binding in 10 (4 male / 6 female) healthy subjects (age range 39 - 70 years, mean age ± standard deviation 53.1 ± 12.5 years); thalamus and midbrain showed an age-dependent increase [63]. Additional validation is needed for the use of a population based input function outside the original study it was developed within, as it may be sensitive to experimental factors such as the speed and shape of the radiotracer bolus administration, the peripheral metabolism in the study specific subject population and the properties of the camera used for the acquisition and of the reconstruction of the imaging data.

A subsequent study of 35 (22 male / 13 female) healthy subjects (age range 19 - 79 years) using the SRTM together with a SVCA6 derived reference tissue input function found increased binding of [^{11}C](*R*)-PK11195 with ageing in frontal lobe, anterior and posterior cingulate cortex, medial inferior temporal lobe, insula, hippocampus, entorhinal cortex, thalamus, parietal and occipital lobes and cerebellum [64]. Thus, Schuitemaker *et al.* concluded that in the absence of plasma input data the use of the cerebellum as reference region in healthy ageing studies was not appropriate [64].

Kumar *et al.* scanned 15 (7 male / 8 female) healthy adults (age range 20 - 49 years, mean age ± standard deviation 29 ± 8.5 years) and 10 (5 male / 5 female) children (age range 1.2 - 17 years, mean age ± standard deviation 8.8 ± 5.2 years) in whom neuro-inflammation

was considered to be unlikely on the basis of all available clinical, radiological, serological and follow-up data [65]. Unsupervised cluster analysis [41] was used to segment the dynamic [^{11}C](*R*)-PK11195 images into $k = 9$ clusters, and the cluster characterised by the TAC with lowest maximal value and fastest washout was used as reference input to the SRTM [65]. BP_{ND} in the cerebellum was found to be higher than that in the frontal-parietal-temporal cortex [65]. There was no significant correlation between BP_{ND} values and age, except for thalamus which showed a trend [65]. In addition to the kinetic analysis with the SRTM, a simplified quantification was also performed using standard uptake values (SUVs) calculated from 5 to 20 minutes scan time [65]. Unlike with BP_{ND}, SUVs for all brain regions were found to be significantly higher in adults than in children and showed a very significant positive correlation with age [65]. The finding of an age-related increase of SUV throughout the brain is consistent with the results of another study by Gulyás *et al.* that used [^{11}C]vinpocetine as TSPO radioligand instead of [^{11}C](*R*)-PK11195 and scanned 6 young normal volunteers (age range 22 - 44 years, mean age ± standard deviation 34.8 ± 5.7 years) and 6 aged normal volunteers (age range 54 - 78 years, mean age ± standard deviation 67.3 ± 7.6 years) [66]. However, age-related increases of SUV in the brain can be the consequence of a variety of causes, raised specific binding to TSPO in brain being only one of them but also changes in perfusion and blood volume with age may be confounders.

As the last paper in this section on age-related changes of TSPO radioligand binding in healthy subjects, the study by Suridjan *et al.* is the only one of the series not relying on a reference tissue input function for tracer kinetic modelling by using a metabolite-corrected plasma input function and a two-tissue compartment model with 5 % vascular contribution [67]. 33 (13 male / 20 female) cognitively normal individuals (age range 19 - 82 years, mean age ± standard deviation 49.09 ± 18.6 years) were scanned on the HRRT for 125 min following the injection of the second generation TSPO radioligand [^{18}F]FEPPA [67]. Genetic analysis revealed 22 HABs, 11 MABs and no LABs [67]. Regression analyses adjusting for genetic status on [^{18}F]FEPPA V_T found no significant effect of age in the hippocampus, temporal and prefrontal [67].

The effect of age on [^{18}F]FEPPA V_T remained not significant even after partial volume effect (PVE) correction [67]. Previously, Schuitemaker *et al.* had found no effect on their results when a partial volume-corrected ordered subset expectation maximization reconstruction algorithm incorporating the point spread function of the ECAT EXACT HR+ camera in the system matrix during reconstruction was compared with standard filtered back projection reconstructed images [64, 68]. Therefore, no impact of PVE correction on TSPO PET data in ageing has been demonstrated yet.

It is important, however, to always bear in mind that any relationship of SRTM derived BP_{ND} with age can only reflect differential effects between the target and reference region. It is not possible to assess absolute levels of specific binding to TSPO in any region of the brain unless a reference external to the brain, that is a plasma input function, is used for quantification. Furthermore, dependent on the choice of the reference input function, pharmacologically meaningless BP_{ND} smaller than zero might be obtained for [^{11}C](*R*)-PK11195 scans with any of the brain reference tissue approaches. This can for example occur

with the cerebellum as an anatomically defined reference region, as the [^{11}C](*R*)-PK11195 binding in the frontal, parietal and temporal cortex of young participants was found to be lower than that in the cerebellum [65], resulting in the possibility of negative BP_{ND} with [^{11}C](*R*)-PK11195 for any of those target regions if a cerebellar reference region input function was used [69].

Summary

Quantification of TSPO in the human brain has proven to be very challenging due to the high expression of TSPO in peripheral organs where the radiotracers are bound specifically, the large contribution of non-specific binding in the brain and the absence of a brain reference region devoid of specific binding. As a consequence it has been difficult to demonstrate and visualise neuro-inflammation in various neurological disorders by TSPO PET imaging and several studies with conflicting or inconclusive findings have been reported. Over time various approaches to overcome these limitations have been proposed by developing methods to obtain a more accurate reference tissue TAC and models that may account for the contribution of signal from the vasculature.

In addition, several new radiotracers for TSPO imaging, for example [^{11}C]PBR28 or ^{18}F-labelled *N*,*N*-diethyl-2-(2-[4-(2-fluoroethoxy)phenyl]-5,7-dimethylpyrazolo[1,5-α]pyrimidine-3-yl)acetamide ([^{18}F]DPA-714) have been developed attempting to reduce non-specific binding and thereby, hopefully, being able to identify the specific signal with higher sensitivity [22, 70]. Most of these second generation TSPO radiotracers turned out to be sensitive to the polymorphism of TSPO resulting in different binding affinities which is addressed by Owen *et al.* in a separate article in this edition. Therefore, their use in human TSPO imaging studies is limited to MABs and HABs as the specific binding in LABs appears to be too small. If patient stratification by TSPO binding affinity is to be avoided in clinical research, and all PET data of a clinical group are to be pooled together irrespective of the TSPO binding status of its members, then specific quantification methods that account and adjust for each subject's TSPO binding affinity are needed for these radiotracers. As seen before with [^{11}C](*R*)-PK11195, data driven methods for the extraction of reference tissue kinetics need to be devised for the newer TSPO radiotracers to avoid blood sampling and increase their acceptance for use in clinical studies.

Acknowledgements

We kindly acknowledge Christian Prenant and Gavin D. Brown for their explanations provided on the radiochemistry, David J. Brooks for the invitation to Århus and the stimulating discussions on [^{11}C](*R*)-PK11195 data analysis there, Federico Roncaroli for his advice on neuropathological data and the European Union's Seventh Framework Programme (FP7/2007-2013) for financial support under the grant agreement HEALTH-F2-2011-278850 (Imaging of Neuroinflammation in Neurodegenerative Diseases) bringing the INMiND consortium together.

Compliance with ethical standards

Conflict of interest: The authors declare no conflicts of interest.

Ethical approval and informed consent: All procedures performed in studies with human participants in which the authors were involved were conducted in accordance with the ethical standards of the institutional and/or national research committee and with the 1964 Helsinki declaration and its later amendments or comparable ethical standards. Informed consent was obtained from all individual participants included in those studies.

This review article does not contain studies with animals performed by any of the authors.

Authors' contributions: R Hinz: Design and content planning of the article; literature search and review; manuscript writing, formatting and editing; correspondence with the editorial office. R Boellaard: Design and content planning of the article; literature search and review; manuscript writing and editing; data processing for the preparation of the figures.

References

[1] Charbonneau P, Syrota A, Crouzel C, Valois JM, Prenant C, Crouzel M (1986) Peripheral-type benzodiazepine receptors in the living heart characterized by positron emission tomography. Circulation 73: 476-483. doi: 10.1161/01.CIR.73.3.476

[2] Bergström M, Mosskin M, Ericson K, Ehrin E, Thorell JO, von Holst H, Norén G, Persson A, Halldin C, Stone-Elander S (1986) Peripheral benzodiazepine binding sites in human gliomas evaluated with positron emission tomography. Acta Radiol Suppl 369: 409-411.

[3] Junck L, Olson JM, Ciliax BJ, Koeppe RA, Watkins GL, Jewett DM, McKeever PE, Wieland DM, Kilbourn MR, Starosta-Rubinstein S, Mancini WR, Kuhl DE, Greenberg HS, Young AB (1989) PET imaging of human gliomas with ligands for the peripheral benzodiazepine binding site. Ann Neurol 26: 752-758. doi: 10.1002/ana.410260611

[4] Ramsay SC, Weiller C, Myers R, Cremer JE, Luthra SK, Lammertsma AA, Frackowiak RS (1992) Monitoring by PET of macrophage accumulation in brain after ischaemic stroke. Lancet 339: 1054-1055. doi: 10.1016/0140-6736(92)90576-O

[5] Blomqvist G, Pauli S, Farde L, Eriksson L, Persson A, Halldin C (1989) Dynamic models of reversible ligand binding. In: Beckers C, Goffinet A, Bol A (eds) Positron emission tomography in clinical research and clinical diagnosis: tracer modelling and radioreceptors. Kluwer Academic Publishers, Dardrecht, The Netherlands, pp 35-44. ISBN 0-7923-0254-0

[6] Cunningham VJ, Hume SP, Price GR, Ahier RG, Cremer JE, Jones AKP (1991) Compartmental analysis of diprenorphine binding to opiate receptors in the rat in vivo and its comparison with equilibrium data in vitro. J Cereb Blood Flow Metab 11: 1-9. doi: 10.1038/jcbfm.1991.1

[7] Lammertsma AA, Bench CJ, Hume SP, Osman S, Gunn K, Brooks DJ, Frackowiak RSJ (1996) Comparison of methods for analysis of clinical [^{11}C]raclopride studies. J Cereb Blood Flow Metab 16: 42-52. doi: 10.1097/00004647-199601000-00005

[8] Lammertsma AA, Hume SP (1996) Simplified reference tissue model for PET receptor studies. Neuroimage 4: 153-158. doi: 10.1006/nimg.1996.0066

[9] Logan J, Fowler JS, Volkow ND, Wang G-J, Ding YS, Alexoff DL (1996) Distribution volume ratios without blood sampling from graphical analysis of PET data. J Cereb Blood Flow Metab 16: 834-840. doi: 10.1097/00004647-199609000-00008

[10] Pike VW, Halldin C, Crouzel C, Barre L, Nutt DJ, Osman S, Shah F, Turton DR, Waters SL (1993) Radioligands for PET studies of central benzodiazepine receptors and PK (peripheral benzodiazepine) binding sites - current status. Nucl Med Biol 20: 503-525. doi: 10.1016/0969-8051(93)90082-6

[11] De Vos F, Dumont F, Santens P, Slegers G, Dierckx R, De Reuck J (1999) High-performance liquid chromatographic determination of [^{11}C]1-(2-chlorophenyl)-*N*-

methyl-*N*-(1-methylpropyl)-3-isoquinoline carboxamide in mouse plasma and tissue and in human plasma. J Chromatogr B Biomed Sci Appl 736: 61-66.

[12] Greuter HNJM, van Ophemert PLB, Luurtsema G, van Berckel BNM, Franssen EJF, Windhorst BD, Lammertsma AA (2005) Optimizing an online SPE-HPLC method for analysis of (*R*)-[^{11}C]1-(2-chlorophenyl)-*N*-methyl-*N*-(1-methylpropyl)-3-isoquinolinecarboxamide [(*R*)-[^{11}C]PK11195] and its metabolites in humans. Nucl Med Biol 32: 307-312. doi: 10.1016/j.nucmedbio.2004.12.005

[13] Shah F, Hume SP, Pike VW, Ashworth S, McDermott J (1994) Synthesis of the enantiomers of [*N*-methyl-^{11}C]PK 11195 and comparison of their behaviours as radioligands for PK binding sites in rats. Nucl Med Biol 21: 573-581. doi: 10.1016/0969-8051(94)90022-1

[14] Jaremko Ł, Jaremko M, Giller K, Becker S, Zweckstetter M (2014) Structure of the mitochondrial translocator protein in complex with a diagnostic ligand. Science 343: 1363-1366. doi: 10.1126/science.1248725

[15] Roivainen A, Någren K, Hirvonen J, Oikonen V, Virsu P, Tolvanen T, Rinne JO (2009) Whole-body distribution and metabolism of [*N*-methyl-^{11}C](*R*)-1-(2-chlorophenyl)-*N*-(1-methylpropyl)-3-isoquinolinecarboxamide in humans; an imaging agent for in vivo assessment of peripheral benzodiazepine receptor activity with positron emission tomography. Eur J Nucl Med Mol Imaging 36: 671-682. doi: 10.1007/s00259-008-1000-1

[16] Jučaite A, Cselényi Z, Arvidsson A, Åhlberg G, Julin P, Varnäs K, Stenkrona P, Andersson J, Halldin C, Farde L (2012) Kinetic analysis and test-retest variability of the radioligand [^{11}C](*R*)-PK11195 binding to TSPO in the human brain - a PET study in control subjects. EJNMMI Res 2: 15. doi: 10.1186/2191-219X-2-15

[17] Lamare F, Hinz R, Gaemperli O, Pugliese F, Mason JC, Spinks TJ, Camici PG, Rimoldi OE (2011) Detection and quantification of large vessel inflammation with ^{11}C-(*R*)-PK11195 PET/CT. J Nucl Med 52: 33-39. doi: 10.2967/jnumed.110.079038

[18] Groom GN, Junck L, Foster NL, Frey KA, Kuhl DE (1995) PET of peripheral benzodiazepine binding sites in the microgliosis of Alzheimer's disease. J Nucl Med 36: 2207-2210.

[19] Rozemuller JM, van der Valk P, Eikelenboom P (1992) Activated microglia and cerebral amyloid deposits in Alzheimer's disease. Res Immunol 143: 646-649. doi: /101016/0923-2494(92)80050-U

[20] Wyss-Coray, T. (2006) Inflammation in Alzheimer disease: driving force, bystander or beneficial response? Nat Med 12: 1005-1015. doi: 10.1038/nm1484

[21] Doble A, Malgouris C, Daniel M, Daniel N, Imbault F, Basbaum A, Uzan A, Gueremy C, Le Fur G (1987) Labelling of peripheral-type benzodiazepine binding sites in human brain with [^{3}H]PK 11195: anatomical and subcellular distribution. Brain Res Bull 18: 49-61. doi: 10.1016/0361-9230(87)90033-5

[22] Owen DR, Guo Q, Kalk NJ, Colasanti A, Kalogiannopoulou D, Dimber R, Lewis YL, Libri V, Barletta J, Ramada-Magalhaes J, Kamalakaran A, Nutt DJ, Passchier J, Matthews PM, Gunn RN, Rabiner EA (2014) Determination of [^{11}C]PBR28 binding potential in vivo: a first human TSPO blocking study. J Cereb Blood Flow Metab 34: 989-994. doi: 10.1038/jcbfm.2014.46

[23] Owen DR, Yeo AJ, Gunn RN, Song K, Wadsworth G, Lewis A, Rhodes C, Pulford DJ, Bennacef I, Parker CA, StJean PL, Cardon LR, Mooser VE, Matthews PM, Rabiner EA, Rubio JP (2012) An 18-kDa translocator protein (TSPO) polymorphism explains differences in binding affinity of the PET radioligand PBR28. J Cereb Blood Flow Metab 32: 1-5. doi: 10.1038/jcbfm.2011.147

[24] Lassen NA, Bartenstein PA, Lammertsma AA, Prevett MC, Turton DR, Luthra SK, Osman S, Bloomfield PM, Jones T, Patsalos PN, O'Connell MT, Duncan JS, Vanggaard Andersen J (1995) Benzodiazepine receptor quantification in vivo in humans using [^{11}C]flumazenil and PET: application of the steady-state principle. J Cereb Blood Flow Metab 15: 152-165. doi: 10.1038/jcbfm.1995.17

[25] Cunningham VJ, Rabiner EA, Slifstein M, Laruelle M, Gunn RN (2010) Measuring drug occupancy in the absence of a reference region: the Lassen plot re-visited. J Cereb Blood Flow Metab 30: 46-50. doi: 10.1038/jcbfm.2009.190

[26] Mintun, M.A.; Raichle, M.E.; Kilbourn, M.R.; Wooten, G.F.; Welch, M.J. (1984) A quantitative model for the in vivo assessment of drug binding sites with positron emission tomography. Ann Neurol 15: 217-227. doi: 10.1002/ana.410150302

[27] Innis, R.B.; Cunningham, V.J.; Delforge, J.; Fujita, M.; Gjedde, A.; Gunn, R.N.; Holden, J.; Houle, S.; Huang, S.-C.; Ichise, M.; Iida, H.; Ito, H.; Kimura, Y.; Koeppe, R.A.; Knudsen, G.M.; Knuuti, J.; Lammertsma, A.A.; Laruelle, M.; Logan, J.; Maguire, R.P.; Mintun, M.A.; Morris, E.D.; Parsey, R.; Price, J.C.; Slifstein, M.; Sossi, V.; Suhara, T.; Votaw, J.R.; Wong, D.F.; Carson, R.E. (2007) Consensus nomenclature for in vivo imaging of reversibly binding radioligands. J. Cereb. Blood Flow Metab. 27, 1533-1539. doi: 10.1038/sj.jcbfm.9600493

[28] Koeppe RA, Holthoff VA, Frey KA, Kilbourn MR, Kuhl DE (1991) Compartmental analysis of [^{11}C]flumazenil kinetics for the estimation of ligand receptor distribution using positron emission tomography. J Cereb Blood Flow Metab 11: 735-744. doi: 10.1038/jcbfm.1991.130

[29] Carson RE, Channing MA, Blasberg RG, Dunn BB, Cohen RM, Rice KC, Herscovitch P (1993) Comparison of bolus and infusion methods for receptor quantitation: application to [^{18}F]cyclofoxy and positron emission tomography. J Cereb Blood Flow Metab 13: 24-42. doi: 10.1038/jcbfm.1993.6

[30] Chapter 5 Equations of radioactive decay and growth (1981) In: Friedlander G, Kennedy JW, Macias ES, Miller JM Nuclear and radiochemistry, 3rd edn. Wiley, New York, pp 191-205

[31] Slifstein M (2008) Revisiting an old issue: the discrepancy between tissue ratio-derived binding parameters and kinetic modeling-derived parameters after a bolus of the serotonin transporter radioligand ^{123}I-ADAM. J Nucl Med 49: 176-178. doi: 10.2967/jnumed.107.046631

[32] Slifstein M, Laruelle M (2001) Models and methods for derivation of *in vivo* neuroreceptor parameters with PET and SPECT reversible radiotracers. Nucl Med Biol 28: 595-608. doi: 10.1016/S0969-8051(01)00214-1

[33] Hanahan D, Weinberg RA (2011) Hallmarks of cancer: the next generation. Cell 144: 646-674. doi: 10.1016/j.cell.2011.02.013

[34] Hanahan D, Weinberg RA (2000) The hallmarks of cancer. Cell 100: 57-70. doi:10.1016/S0092-8674(00)81683-9

[35] Cagnin A, Brooks DJ, Kennedy AM, Gunn RN, Myers R, Turkheimer FE, Jones T, Banati RB (2001) In-vivo measurement of activated microglia in dementia. Lancet 358: 461-467. doi: 10.1016/S0140-6736(01)05625-2

[36] Gunn RN, Lammertsma AA, Hume SP, Cunningham VJ (1997) Parametric imaging of ligand-receptor binding in PET using a simplified reference region model. Neuromage 6: 279-287. doi: 101006/nimg19970303

[37] Herholz K, Patlak CS (1987) The influence of tissue heterogeneity on results of fitting nonlinear model equations to regional tracer uptake curves: with an application to compartmental models used in positron emission tomography. J Cereb Blood Flow Metab 7: 214-229. doi: 10.1038/jcbfm.1987.47

[38] Mahalanobis PC (1936) On the generalised distance in statistics. Proceedings of the National Institute of Science of India 12: 49-55.

[39] Rousseeuw PJ (1987) Silhouettes: a graphical aid to the interpretation and validation of cluster analysis. J Comput Appl Math 20: 53-65. doi: 10.1016/0377-0427(87)90125-7

[40] O'Sullivan F (1993) Imaging radiotracer model parameters in PET: a mixture analysis approach. IEEE Trans Med Imaging 12: 399-412. doi: 10.1109/42.241867

[41] Ashburner J, Haslam J, Taylor C, Cunningham VJ, Jones T (1996) A cluster analysis approach for the characterization of dynamic PET data. In: Myers R, Cunningham V, Bailey D, Jones T (eds) Quantification of brain function using PET. Academic Press, San Diego, California, pp 301-306. ISBN 0-12-389760-2 doi: 10.1016/B978-012389760-2/50061-X

[42] Myers R, Gunn RN, Cunningham VJ, Banati RB, Jones T (1999) Cluster analysis and the reference tissue model in the analysis of clinical [^{11}C]PK11195 PET. J Cereb Blood Flow Metab 19: S789.

[43] Cagnin A, Myers R, Gunn RN, Turkheimer FE, Cunningham VJ, Brooks DJ, Jones T, Banati RB (2000) Imaging activated microglia in the aging human brain. In: Gjedde A, Hansen SB, Knudsen GM, Paulson OB (eds) Physiological imaging of the brain with PET. Academic Press, San Diego, California, pp 361-367. ISBN 0-12-285751-8

[44] Banati RB, Newcombe J, Gunn RN, Cagnin A, Turkheimer F, Heppner F, Price G, Wegner F, Giovannoni G, Miller DH, Perkin GD, Smith T, Hewson AK, Bydder G, Kreutzberg GW, Jones T, Cuzner ML, Myers R (2000) The peripheral benzodiazepine binding site in the brain in multiple sclerosis: quantitative in vivo imaging of microglia as a measure of disease activity. Brain 123: 2321 - 2337. dx: 10.1093/brain/123.11.2321

[45] Kropholler MA, Boellaard R, van Berckel BN, Schuitemaker A, Kloet RW, Lubberink MJ, Jonker C, Scheltens P, Lammertsma AA (2007) Evaluation of reference regions for (*R*)-[^{11}C]PK11195 studies in Alzheimer's disease and mild cognitive impairment. J Cereb Blood Flow Metab 27: 1965-1974. doi: 10.1038/sj.jcbfm.9600488

[46] Turkheimer FE, Edison P, Pavese N, Roncaroli F, Anderson AN, Hammers A, Gerhard A, Hinz R Tai YF, Brooks DJ (2007) Reference and target region modeling of [^{11}C]-(*R*)-PK11195 brain studies. J Nucl Med 48: 158-167.

[47] Chen J, Gunn S, Nixon M, Myers R, Gunn R (2000) A supervised method for PET reference region extraction. In: Arridge S, Todd-Pokropek A (eds) Medical image understanding and analysis MIUA 2000: proceedings of the fourth annual conference. University College London, UK, pp 179-182. ISBN 1-901725-11-1

[48] Lawson CL, Hanson RJ (1995) Solving least squares problems. Society for Industrial and Applied Mathematics (SIAM), Philadelphia. ISBN 0-89871-356-0

[49] Cunningham VJ, Jones T (1993) Spectral analysis of dynamic PET studies. J Cereb Blood Flow Metab 13: 15 - 23. doi: 10.1038/jcbfm.1993.5

[50] Hinz R, Jones M, Bloomfield PM, Boellaard R, Turkheimer FE, Tyrrell PJ (2008) Reference tissue kinetics extraction from [^{11}C]-(*R*)-PK11195 scans on the High Resolution Research Tomograph (HRRT). Neuroimage 41, suppl. 2: T65. doi:10.1016/j.neuroimage.2008.04.035

[51] Drake C, Boutin H, Jones MS, Denes A, McColl BW, Selvarajah JR, Hulme S, Georgiou RF, Hinz R, Gerhard A, Vail A, Prenant C, Julyan P, Maroy R, Brown G, Smigova A, Herholz K, Kassiou M, Crossman D, Francis S, Proctor SD, Russell JC, Hopkins SJ, Tyrrell PJ, Rothwell NJ, Allan SM (2011) Brain inflammation is induced by co-morbidities and risk factors for stroke. Brain Behav Immun 25: 1113-1122. doi: 10.1016/j.bbi.2011.02.008

[52] Boellaard R, Turkheimer FE, Hinz R, Schuitemaker A, Scheltens P, van Berckel BNM, Lammertsma AA (2008) Performance of a modified supervised cluster algorithm for extracting reference region input functions from (*R*)-[^{11}C]PK11195 brain PET studies. IEEE Nuclear Science Symposium Conference Record: 5400-5402. doi: 10.1109/NSSMIC.2008.4774453

[53] Folkersma H, Boellaard R, Vandertop WP, Kloet RW, Lubberink M, Lammertsma AA, van Berckel BNM (2009) Reference tissue models and blood-brain barrier disruption: lessons from (*R*)-[^{11}C]PK11195 in traumatic brain injury. J Nucl Med 50: 1975-1979. doi: 10.2967/jnumed.109.067512

[54] Costes N, Blanc C, Bouillot C, Yankam Njiwa J, Bolbos R, Bouvard S, Chauveau F, Le Bars D, Turkheimer FE, Hammers A (2013) Supervised clustering for determining a reference region for [^{11}C]PK11195 PET: adaptation to rat PET studies. 11th International Conference on Quantification of Brain Function with PET (BrainPET'13), Shanghai, China, 20 - 23 May, 2013.

[55] Su Z, Herholz K, Gerhard A, Roncaroli F, Du Plessis D, Jackson A, Turkheimer F, Hinz R (2013) [^{11}C]-(*R*)PK11195 tracer kinetics in the brain of glioma patients and a comparison of two referencing approaches. Eur J Nucl Med Mol Imaging 40: 1406-1419. doi: 10.1007/s00259-013-2447-2

[56] Holland GP, Hunter JA, Su Z, Kobylecki C, Gerhard A, Hinz R (2014) Extraction of reference tissue kinetics from [^{11}C]-(*R*)PK11195 brain scans: limits of applications. 10th International Symposium on Functional Neuroreceptor Mapping (NRM) of the Living Brain, Egmond aan Zee, the Netherlands, 21 - 24 May, 2014. Abstract Book, 117. http://www.vumc.nl/afdelingen-themas/50095/69479/Program-Abstractbook.pdf?version=1

[57] Yaqub M, van Berckel BN, Schuitemaker A, Hinz R, Turkheimer FE, Tomasi G, Lammertsma AA, Boellaard R (2012) Optimization of supervised cluster analysis for extracting reference tissue input curves in (*R*)-[^{11}C]PK11195 brain PET studies. J Cereb Blood Flow Metab 32: 1600-1608. doi: 10.1038/jcbfm.2012.59

[58] Kropholler MA, Boellaard R, Schuitemaker A, van Berckel BN, Luurtsema G, Windhorst AD, Lammertsma AA (2005) Development of a tracer kinetic plasma input model for (*R*)-[^{11}C]PK11195 brain studies. J Cereb Blood Flow Metab 25: 842-851. doi: 10.1038/sj.jcbfm.9600092

[59] Kropholler MA, Boellaard R, Schuitemaker A, Folkersma H, van Berckel BN, Lammertsma AA (2006) Evaluation of reference tissue models for the analysis of [^{11}C](*R*)-PK11195 studies. J Cereb Blood Flow Metab 26: 1431-1441. doi: 10.1038/sj.jcbfm.9600289

[60] Tomasi G.; Edison P.; Bertoldo A.; Roncaroli F.; Singh P.; Gerhard A.; Cobelli C.; Brooks D.J.; Turkheimer F.E. (2008) Novel reference region model reveals increased microglial and reduced vascular binding of ^{11}C-(*R*)-PK11195 in patients with Alzheimer's disease. J Nucl Med 49: 1249-1256. doi: 10.2967/jnumed.108.050583

[61] Gunn RN, Sargent PA, Bench CJ, Rabiner EA, Osman S, Pike VW, Hume SP, Grasby PM, Lammertsma AA Tracer kinetic modeling of the 5-HT$_{1A}$ receptor ligand [*carbonyl*-^{11}C]WAY- 100635 for PET. Neuroimage 8: 426-440. doi: 10.1006/nimg.1998.0379

[62] Rizzo G Veronese M Tonietto M Zanotti-Fregonara P Turkheimer FE Bertoldo A (2014) Kinetic modeling without accounting for the vascular component impairs the quantification of [^{11}C]PBR28 brain PET data. J Cereb Blood Flow Metab. 34 1060–1069. doi: 10.1038/jcbfm.2014.55

[63] Ouchi Y, Yoshikawa E, Sekine Y, Futatsubashi M, Kanno T, Ogusu T, Torizuka T (2005) Microglial activation and dopamine terminal loss in early Parkinson's disease. Ann Neurol 57: 168 - 175. doi: 10.1002/ana.20338

[64] Schuitemaker A, van der Doef TF, Boellaard R, van der Flier WM, Yaqub M, Windhorst AD, Barkhof F, Jonker C, Kloet RW, Lammertsma AA, Scheltens P, van Berckel BN (2012) Microglial activation in healthy aging. Neurobiol Aging 33: 1067 - 1072. doi: 10.1016/j.neurobiolaging.2010.09.016

[65] Kumar A, Muzik O, Shandal V, Chugani D, Chakraborty P, Chugani HT (2012) Evaluation of age-related changes in translocator protein (TSPO) in human brain using ^{11}C-[R]-PK11195 PET. J Neuroinflammation 9: 232. doi: 10.1186/1742-2094-9-232

[66] Gulyás B, Vas A, Tóth M, Takano A, Varrone A, Cselényi Z, Schain M, Mattsson P, Halldin C (2011) Age and disease related changes in the translocator protein (TSPO) system in the human brain: positron emission tomography measurements with [^{11}C]vinpocetine. Neuroimage 56: 1111 - 1121. doi: 10.1016/j.neuroimage.2011.02.020

[67] Suridjan, I.; Rusjan, P.M.; Voineskos, A.N.; Selvanathan, T.; Setiawan, E.; Strafella, A.P.; Wilson, A.A.; Meyer, J.H.; Houle, S.; Mizrahi, R. (2014) Neuroinflammation in healthy aging: A PET study using a novel Translocator Protein 18kDa (TSPO) radioligand, [^{18}F]-FEPPA. Neuroimage 84: 868 - 875. doi: 10.1016/j.neuroimage.2013.09.021

[68] Schuitemaker A, Kropholler MA, Boellaard R, van der Flier WM, Kloet RW, van der Doef TF, Knol DL, Windhorst AD, Luurtsema G, Barkhof F, Jonker C, Lammertsma AA, Scheltens P, van Berckel BN (2013) Microglial activation in Alzheimer's disease: an (*R*)-[^{11}C]PK11195 positron emission tomography study. Neurobiol Aging 34: 128 - 136. doi: 10.1016/j.neurobiolaging.2012.04.021

[69] Hunter HJA, Hinz R, Gerhard A, Talbot PS, Su Z, Holland G, Hopkins SJ, Griffiths CEM, Kleyn CE (2015) Brain inflammation and psoriasis: a [^{11}C]-(*R*)-PK11195 positron emission tomography study. Br J Dermatol. doi: 10.1111/bjd.13788

[70] Golla SSV, Boellaard R, Oikonen V, Hoffmann A, van Berckel BNM, Windhorst AD, Virta J, Haaparanta-Solin M, Luoto P, Savisto N, Solin O, Valencia R, Thiele A, Eriksson J, Schuit RC, Lammertsma AA, Rinne JO (2015) Quantification of [^{18}F]DPA-714 binding in the human brain: initial studies in healthy controls and Alzheimer's disease patients. J Cereb Blood Flow Metab 35: 766 - 772. doi: 10.1038/jcbfm.2014.261

Figure captions

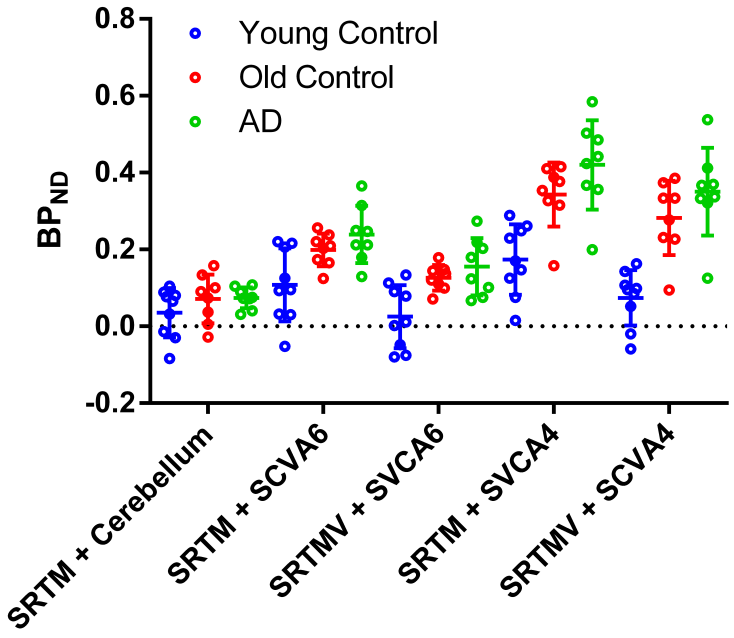

Fig 1 Regional [^{11}C](*R*)-PK11195 binding potentials BP_{ND} of the bilateral thalamus obtained in cohorts of 9 young controls (blue circles), 8 old controls (red circles) and 8 Alzheimer's Disease (AD) patients (green circles) obtained with different reference tissue models (SRTM: simplified reference tissue model, SRTMV: simplified reference tissue model with vascular component) and input functions (anatomically defined Cerebellum, SVCA6: supervised cluster analysis with six kinetic classes, SVCA4: supervised cluster analysis with four kinetic classes and brain mask) [57]. Horizontal lines represent the group mean ± one standard deviation. Though thalamic nuclei are among the structures in the normal human brain *post mortem* with the highest densities of [^{3}H]PK11195 specific binding [21], several individual BP_{ND} estimates were still negative mostly in young controls with a cerebellar reference input. Several [^{11}C](*R*)-PK11195 studies using different variants of cluster analysis to extract a reference input function reported higher BP_{ND} in the thalamus of older controls (red) compared with younger controls (blue) [35, 43, 63 - 65]. In contrast, dementia studies included here found no statistically significant group difference of the BP_{ND} in the thalamus between AD patients (green) and age-matched controls (red) [18, 35, 68].

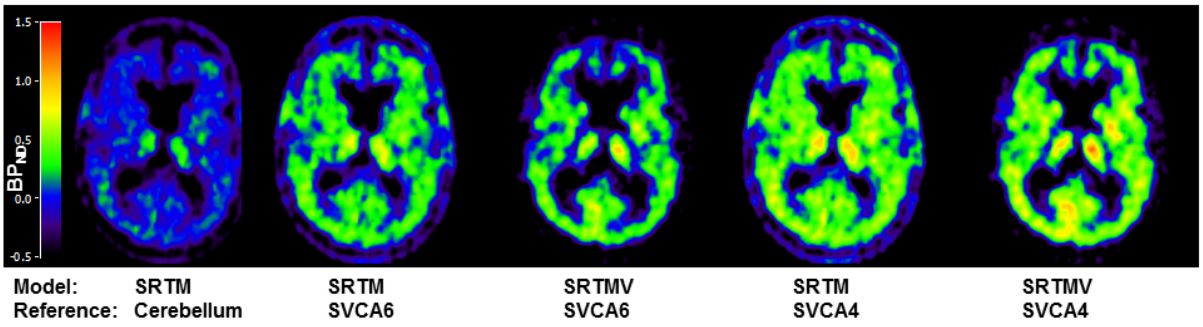

Fig 2 Transverse slice through the parametric maps of [^{11}C](*R*)-PK11195 binding potential BP_{ND} of a single subject with Alzheimer's Disease generated with different reference tissue models (SRTM: simplified reference tissue model, SRTMV: simplified reference tissue model with vascular component) and input functions (anatomically defined Cerebellum, SVCA6: supervised cluster analysis with six kinetic classes, SVCA4: supervised cluster analysis with four kinetic classes and brain mask) [57].